A *Sleeping Beauty* mutagenesis screen reveals a tumor suppressor role for *Ncoa2/Src-2* in liver cancer

Kathryn A. O'Donnell[a,b,1,2], Vincent W. Keng[c,d,e], Brian York[f], Erin L. Reineke[f], Daekwan Seo[g], Danhua Fan[c,h], Kevin A. T. Silverstein[c,h], Christina T. Schrum[a,b], Wei Rose Xie[a,b,3], Loris Mularoni[i,j], Sarah J. Wheelan[i,j], Michael S. Torbenson[k], Bert W. O'Malley[f], David A. Largaespada[c,d,e], and Jef D. Boeke[a,b,i,2]

Departments of [a]Molecular Biology and Genetics, [i]Oncology, [j]Division of Biostatistics and Bioinformatics, and [k]Pathology and [b]The High Throughput Biology Center, The Johns Hopkins University School of Medicine, Baltimore, MD 21205; [c]Masonic Cancer Center, [d]Department of Genetics, Cell Biology, and Development, [e]Center for Genome Engineering, and [h]Biostatistics and Bioinformatics Core, University of Minnesota, Minneapolis, MN 55455; [f]Department of Molecular and Cellular Biology, Baylor College of Medicine, Houston, TX 77030; and [g]Laboratory of Experimental Carcinogenesis, Center for Cancer Research, National Cancer Institute, National Institutes of Health, Bethesda, MD, 20892

Edited by Harold Varmus, National Cancer Institute, Bethesda, MD, and approved March 23, 2012 (received for review September 21, 2011)

The *Sleeping Beauty* (*SB*) transposon mutagenesis system is a powerful tool that facilitates the discovery of mutations that accelerate tumorigenesis. In this study, we sought to identify mutations that cooperate with *MYC*, one of the most commonly dysregulated genes in human malignancy. We performed a forward genetic screen with a mouse model of MYC-induced liver cancer using SB-mediated mutagenesis. We sequenced insertions in 63 liver tumor nodules and identified at least 16 genes/loci that contribute to accelerated tumor development. RNAi-mediated knockdown in a liver progenitor cell line further validate three of these genes, *Ncoa2/Src-2, Zfx,* and *Dtnb,* as tumor suppressors in liver cancer. Moreover, deletion of *Ncoa2/Src-2* in mice predisposes to diethylnitrosamine-induced liver tumorigenesis. These findings reveal genes and pathways that functionally restrain MYC-mediated liver tumorigenesis and therefore may provide targets for cancer therapy.

cancer gene identification | mouse models of cancer | Myc oncogene | hepatocellular carcinoma

Transposable elements (TEs) are powerful genetic tools that are widely used in insertional mutagenesis screens because of the facile identification of transposon-induced mutations. The application of transposon-based approaches to cancer gene identification provides opportunities to study the consequences of specific mutations in the context of tumor cell initiation, progression, and maintenance in well-defined, genetically engineered mouse models. *Sleeping Beauty* (*SB*), a member of the Tc1/mariner superfamily of DNA transposons, is highly active in mammalian cells (1). A growing body of evidence has demonstrated that *SB* is an efficient tool for cancer gene discovery when used in forward genetic screens in mice (2, 3).

The *SB* system is based on the use of two transgenic mouse lines, one harboring a transposase and the other with a concatemerized mutagenic transposon containing sequences that can disrupt gene function through either gain-of-function or loss-of-function mechanisms. The transposase binds to the transposon ends and catalyzes its mobilization to new sites. The effect of ubiquitous transposition in mice is the development of T-cell leukemia and brain tumors (3, 4). In contrast, restricted expression of *SB* transposase accelerates fibrosarcoma development in $p19^{Arf\ -/-}$ mice (2).

Recently, this approach has been modified through the conditional activation of the SB transposase in specific tissues using Cre/LoxP technology (5, 6). In one of these studies, an *SB* screen identified 19 genes that accelerate liver cancer induced by expression of a dominant-negative *Trp53* transgene. However, the *SB* system has not been used previously to identify genes that cooperate with oncogenes that initiate liver tumorigenesis.

Hepatocellular carcinoma (HCC) is the fifth most common solid tumor worldwide and is the third leading cause of death from cancer (7, 8). In the majority of cases, it occurs in a setting of chronic inflammation or cirrhosis. Although numerous genomic alterations have been documented in liver cancer, the key genetic alterations that drive hepatocellular transformation remain poorly understood. Nevertheless, a unifying feature of human HCC is amplification or overexpression of the *MYC* oncogene (8, 9). The need to identify genetic abnormalities and to understand better how they drive cellular transformation is underscored by the fact that HCC often is diagnosed at an advanced stage when no longer amenable to curative therapies. Thus, the identification of critical genes and pathways dysregulated in HCC may accelerate the development of therapeutic strategies.

We sought to identify mutations that cooperate with *MYC*, one of the most commonly dysregulated oncogenes in human malignancy. We bred mice containing the *SB* DNA transposon vector transgene and an *SB* transposase transgene to a well-characterized model of *MYC*-induced liver cancer (10–12). We hypothesized that mice harboring the active SB transposon would accumulate mutations that accelerate the rate of tumorigenesis in this sensitized liver tumor model. A cohort of quadruple-transgenic mice was generated, each containing the *SB* transposon harboring a gene trap element (T2/Onc), a ubiquitously expressed transposase (*Rosa26-SB11*), a tetracycline (tet)-repressible *MYC* transgene (tet-*o*-*MYC*), and a liver-specific tet-transactivator (LAPtTA) protein. Triple-transgenic mice lacking either the transposon or transposase served as a control cohort. We observed a significant acceleration of tumorigenesis in quadruple-transgenic mice compared with control animals. Sequencing of tumors from quadruple-transgenic animals identified at least 16 genes/loci associated with accelerated liver tumor development. Validation studies in mouse liver progenitor cells (13–15) confirmed that knockdown of selected genes promotes tumorigenesis in xenograft assays. Finally, we further characterized one of the genes, *Nuclear receptor coactivator2* (*Ncoa2*/*Src-2,* hereafter referred to as "*Ncoa2*"), which facilitates transcription of *Glucose 6 phosphatase* (*G6pc*) and thus plays a critical role in

Author contributions: K.A.O., D.A.L., and J.D.B. designed research; K.A.O., V.W.K., B.Y., E.L.R., C.T.S., W.R.X., and B.W.O. performed research; M.S.T. and D.A.L. contributed new reagents/analytic tools; K.A.O., B.Y., E.L.R., D.S., D.F., K.A.S., L.M., and S.J.W. analyzed data; and K.A.O. and J.D.B. wrote the paper.

The authors declare no conflict of interest.

This article is a PNAS Direct Submission.

Data deposition: The sequences from this study have been submitted to the National Center for Biotechnology Information (NCBI) Short Read Archive, http://www.ncbi.nlm.nih.gov/sra (accession no. SRA051795.1).

[1]Present address: Department of Molecular Biology, University of Texas Southwestern Medical Center, Dallas, TX 75390.

[2]To whom correspondence may be addressed. E-mail: Kathryn.ODonnell@UTSouthwestern.edu or jboeke@jhmi.edu.

[3]Present address: Department of Molecular and Human Genetics, Graduate Program in Cell and Molecular Biology, Baylor College of Medicine, Houston, TX 77030.

See Author Summary on page 7966 (volume 109, number 21).

This article contains supporting information online at www.pnas.org/lookup/suppl/doi:10.1073/pnas.1115433109/-/DCSupplemental.

mammalian glucose availability. We find that low levels of *NCOA2* and *G6PC* expression in HCC patients are associated with poor survival. Moreover, deletion of *Ncoa2* in mice promotes diethylnitrosamine (DEN)-induced liver tumorigenesis. These findings reveal genes that function to restrain *MYC*-induced liver tumorigenesis in multiple model systems, thereby revealing pathways that may be attractive targets for therapy.

Results

SB-Induced Mutations Accelerate Tumor Development in tet-o-MYC; LAPtTA Mice. We used a previously described model of liver cancer in which mice harboring tet-*o-MYC* are crossed with mice expressing the tet-transactivator protein (tTA) driven by the liver-activator protein (LAP) promoter (10–12). Upon removal of doxycycline, double-transgenic animals express *MYC* specifically in the liver and subsequently develop liver tumors that resemble HCC. These mice served as a sensitized model of HCC.

Before proceeding with the transposon-mediated forward genetic screen, we performed a control experiment to determine tumor latency in the *MYC* liver model. The purpose of this experiment was twofold. First, the control experiment allowed us to distinguish early-developing tumors that form because of *SB* insertions from tumors that develop at baseline in tet-*o-MYC*; LAPtTA mice. Second, this experiment also provided a control for genetic background, because the *SB* mice are maintained on a mixed FVB/N and C57BL/6J background. We first crossed tet-*o-MYC*; LAPtTA mice, which are maintained on an FVB/N background, with C57BL/6J WT mice. Because of the positioning of the *MYC* transgene on the Y chromosome, only males are assessed in this model. *MYC* was induced when progeny reached 6 wk of age; mice then were dissected and scored for tumors each week from week 11 to week 22 (Fig. S1). Double-transgenic mice developed liver tumors no earlier than 13 wk on this mixed genetic background. Based on these results, we elected to analyze all mice before 16 wk of age, a time point at which liver tumor burden is low in tet-*o-MYC*; LAPtTA mice (Fig. S1).

We bred mice containing the *SB* DNA transposon transgene to the *MYC*-induced liver tumor model. (The crossing scheme is depicted in Fig. S2*A* and the mutagenic transposon is depicted in Fig. S2*B*.)Transposase expression in liver had been demonstrated previously in *Rosa26-SB11* mice (4). We hypothesized that mice harboring an active *SB* transposon would accumulate mutations that accelerate rates of liver tumorigenesis. An experimental cohort of quadruple-transgenic mice was generated, each containing the *SB* transposon harboring a mutagenic gene trap (T2/Onc), a ubiquitously expressed transposase (*Rosa26-SB11*), tet-o-*MYC*, and LAPtTA. We also generated a triple-transgenic control cohort lacking either the transposon or transposase. Doxycycline was withdrawn at 6 wk, and animals were monitored by palpation every 2 or 3 d for early-developing tumors. All animals were euthanized before 16 wk, by which time only 29% of triple-transgenic animals had developed liver tumors (Fig. 1 *A* and *B* and Tables S1 and S2). In contrast, 65% of the quadruple-transgenic mice developed liver tumors by this time point ($P < 0.003$) (Fig. 1*B*).

To confirm T2/Onc transgene concatemer mobilization, we performed a PCR excision assay on liver tumor genomic DNA (gDNA) isolated from quadruple-transgenic and control mice. We verified excision of the transgene in all liver tumors examined (Fig. 1*C*). In contrast, excision of T2/Onc was not observed in a triple-transgenic control animal lacking *Rosa26-SB11* transposase (Fig. 1*C*). We dissected 63 liver tumors from 24 quadruple-transgenic animals (representative pictures of multifocal tumors are shown in Fig. 1*D*). The gross morphology as well as the age of onset of these tumors is distinct from those observed in $Trp53^{-/-}$ mice by Keng et al. (5). Histological analysis confirmed that these tumors resembled human HCC (Fig. 1*D*).

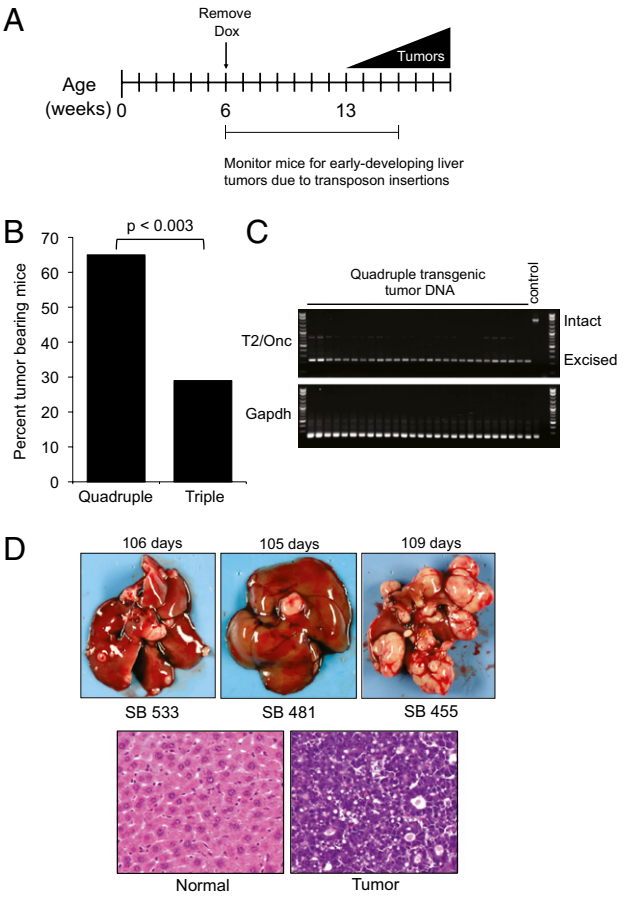

Fig. 1. Acceleration of liver tumorigenesis in tet-*o-Myc;* LAPtTA mice with the *SB* transposon mutagenesis system. (*A*) Time-line of the *SB* mutagenesis screen. Dox, doxycycline. (*B*) Quantification of percentage of quadruple-transgenic (experimental) and triple-transgenic (control) animals that developed liver tumors at time of dissection. $n = 37$ quadruple-transgenic mice; $n = 34$ for triple-transgenic mice. A χ^2 statistic was used for evaluating statistical significance. (*C*) Excision PCR assay demonstrating evidence of transposon (T2/Onc) excision in liver tumors from quadruple-transgenic animals. A T2/Onc (control) animal lacking the *Rosa26-SB11* transposase is also shown. The intact donor T2/Onc amplicon is 2.2 kb, and the excised PCR amplicon is 225 bp. *Gapdh* serves as a control for equal loading of template gDNA. (*D*) (*Upper*) Representative images of multifocal liver tumors from quadruple-transgenic animals. (*Lower*) Histology of normal liver (*Left*) and tumor (*Right*) using H&E staining.

Identification of Common Insertion Sites in Liver Tumors. To identify mutations that cooperate with *MYC* in the development of accelerated liver tumors, common insertion sites (CISs) were identified by sequencing tumors from quadruple-transgenic mice. We first performed ligation-mediated PCR with 63 liver tumor gDNA samples (Fig. S3) followed by 454 pyrosequencing. More than 90,000 individual sequencing reads were generated, of which 98.6% matched to barcodes that were incorporated into the ligation-mediated PCR. *SB* has a strong tendency to favor transposition to sites adjacent to the donor concatemer, a phenomenon termed "local hopping" (16). To control stringently for this bias, we initially excluded insertions that mapped to the same chromosome as the T2/Onc donor concatemer (chromosome 15). We further eliminated insertions that did not map to the canonical TA dinucleotide *SB* insertion site. We then merged all insertions that mapped to the same nucleotide from the same tumor and analyzed a total of 2,090 nonredundant insertions.

The CISs represent potential tumor-modifier genes and are defined by the presence of *SB* insertions at these sites significantly more frequently than would be predicted by random chance. Using

Monte Carlo simulation analysis (5, 6), we defined a statistically significant CIS as a region in the genome with three or more *SB* insertions within a 30-kb window or four or more insertions within 155 kb. Initially, we identified 23 CISs that fit these criteria. Nine of these CISs occurred at the same nucleotide in different tumors from the same mouse and seven were eliminated from consideration as early-occurring passenger insertions less likely to be related to tumor development. Two of these CISs, *Zfp189* and *Bcl9*, remain on the list, because they exhibited concordance with human tumor data. The remaining 14 genes/loci defined by CISs in *MYC*-induced liver tumors are shown in Table 1, along with two others discovered as outlined below.

Consistent with previous studies, we find that genome-level integration of *SB* with respect to genes and intergenic regions is fairly random overall (Fig. S4*A*) (17–19). As expected, we observe the greatest number of insertions clustering around the T2/Onc transgene concatemer on chromosome 15 (Fig. S4*B*). Upon closer inspection of transposon integrations on this chromosome, we identified two additional genes as potential CISs that initially were excluded. These CISs correspond to the *Growth Hormone Receptor* (*Ghr*) and *Nuclear Factor (erythroid-derived 2)* genes (Fig. S4*B* and Table 1). Because these genes are located many megabases from the donor transgene, these transposon insertions cannot be explained solely by local hopping. Moreover, *GHR* was implicated previously in human liver cancer (20).

Insertions in candidate liver cancer genes identified in our screen are shown in Fig. 2*A* and Fig. S5*A*. Two examples are the *Nuclear receptor coactivator2* (*Ncoa2*) and the *Zinc finger transcription factor* (*Zfx*). Insertions in these candidates are distributed randomly throughout the gene and occur in either a sense or antisense orientation. Thus, these insertions are likely to disrupt gene function. To confirm transposon integrations in *Ncoa2*, we performed PCR assays with a gene-specific primer and a T2/Onc primer. In each case, we observed the *SB* insertion in liver tumor gDNA but not in tail gDNA from a C57BL/6J wild-type animal (Fig. 2*B*).

It has been demonstrated previously that *Ncoa2*, a member of the p160 family of transcriptional coactivators, modulates expression of *Glucose 6 phosphatase* (encoding G6Pase) and other important genes by acting in concert with nuclear receptors such as RORα (21, 22). We measured mRNA expression levels of *Ncoa2* and *G6pc* in four liver tumors with *Ncoa2* insertions. Tumors with *SB* insertions exhibited a reduction of both *Ncoa2* and its target *G6pc* mRNA levels (Fig. 2*C*). In contrast, tumors lacking *SB* insertions in *Ncoa2* had normal or elevated expression of this gene (Fig. S6), demonstrating that *Ncoa2* levels are not naturally lower in the cell of origin of HCC in this model.

_SB_ Insertions in Lymphomas Are Distinct from Liver Tumor Insertions. Twenty-nine percent of the quadruple-transgenic animals (11 of 37) developed lymphomas before 16 wk of age, whereas none of the triple-transgenic animals exhibited signs of hematopoietic disease. This result was not unexpected, because T2/Onc; *Rosa26-SB11* mice are known to develop lymphoma and high-grade gliomas on a wild-type genetic background (4). Seven of these 11 quadruple-transgenic animals developed both liver tumors and lymphomas. To distinguish liver tumor-specific insertions from lymphoma-specific insertions in these seven mice, we performed ligation-mediated PCR with spleen gDNA and then sequenced *SB* insertions in these samples. Similar to our analysis with liver tumor *SB* insertions, we searched for CISs that occur at a greater frequency than would be predicted by random chance. We identified 11 genes defined as CISs in these lymphomas (Table S3). Despite the small number of lymphomas analyzed, two of the genes with *SB* insertions, *Myb* and *Erg*, had been found previously as CISs that contribute to leukemias/lymphomas in a larger cohort of 58 T2/Onc; *Rosa26-SB11* animals (4). In contrast, none of the lymphoma CIS genes from the Collier et al. study (4) overlapped with liver CIS genes identified in the present study. Interestingly, the only CIS that overlapped between our lymphoma- and liver tumor-sequencing datasets was *Ncoa2* (Fig. S5*B*). This finding underscores the potential significance of this gene in *MYC*-induced tumorigenesis in multiple settings. Consistent with this, we observed a robust increase in MYC protein levels in *SB*-induced lymphomas compared with normal spleen samples from control animals (Fig. S7). Although the source of elevated MYC in these tumors remains to be determined, it may derive from either the endogenous or transgenic loci.

Functional Validation of CIS Genes Implicates *Ncoa2, Zfx,* and *Dtnb* as Tumor Suppressors. To validate functionally the tumor-suppressor activity of several of the CISs that we identified in our *SB* screen

Table 1. Common insertion sites in early-developing liver tumors

Chromosome	Gene Name	Gene Description	Range (bp)	No. of Tumors	No. of Independent insertion positions
1	*Ncoa2*	Nuclear receptor coactivator 2	117102	7	7
X	*Zfx*	Zinc finger protein X-linked	34704	7	4
11	*Sfi1*	Sfi 1 homolog, spindle assembly associated	51613	3	4
6	*Snd1*	Staphylococcal nuclease and tudor domain containing 1	166208	6	4
1	*AC102110.8*	Putative uncharacterized protein	32748	3	3
1	*Rc3h1*	RING CCCH (C3H) domains 1	158362	3	3
10	*Ctnna3*	Catenin (cadherin associated protein), alpha 3	166868	5	7
3	*AC123647.9*	Uncharacterized protein	103926	4	2
8	*AC171318.3*	Putative uncharacterized protein	153010	4	2
8	*Atbf1/Zfhx3*	AT-motif binding factor 1 (Zinc finger homeobox 3 gene)	161502	4	4
12	*Dtnb*	Dystrobrevin, beta	20080	2	3
2	*AL837506.3-202*	Uncharacterized protein	4508	3	3
4	*Zfp189*	Zinc finger protein 189	34918	3	3
4	*Dnajc6*	DnaJ (Hsp40) homolog, subfamily C, member 6	13890	2	2
18	*Zfp608*	Zinc finger protein 608	1	3	1
3	*Bcl9*	B-cell CLL/lymphoma 9	1	4	1
15	*Nfe2*	Nuclear factor erythroid-derived 2	4708	7	7
15	*Ghr*	Growth hormone receptor	259059	7	7

Common insertion sites in liver tumors from quadruple-transgenic mice defined using Monte Carlo simulation analysis. Independent insertions refer to nonredundant insertions. The CISs below the black line represent genes with insertions at the same nucleotide in tumors from the same mouse or were located on chromosome 15. These CISs remain on the list because their expression showed concordance with HCC data.

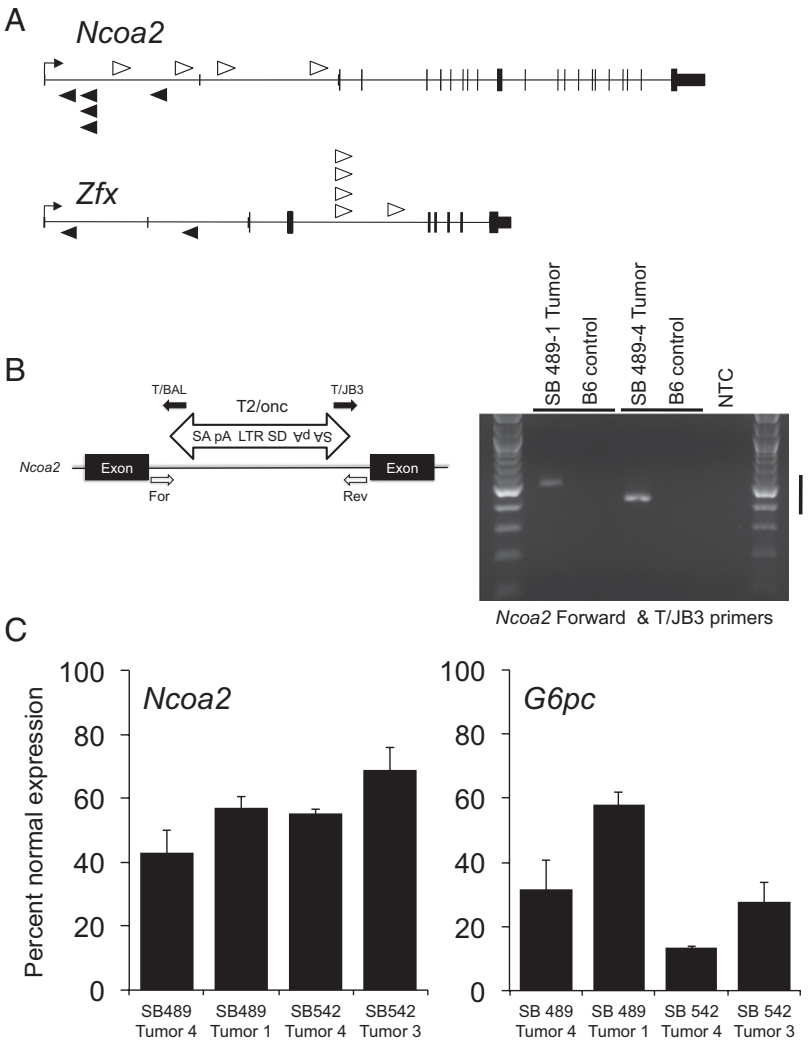

Fig. 2. Transposon insertions in *Ncoa2* and *Zfx* associated with accelerated liver tumorigenesis. (*A*) Schematic representation of *SB* transposon insertions into *Ncoa2* and *Zfx*. White arrowheads represent T2/Onc insertions in the sense orientation relative to target genes. Black arrowheads represent antisense-oriented insertions. The height of protein-coding exons is taller than the untranslated sequences for each gene. (*B*) Validation of *SB* transposon insertions in quadruple-transgenic liver tumors. PCR genotyping was performed using genomic DNA isolated from individual liver tumor nodules. For each insertion, one endogenous primer [forward (For) or reverse (Rev)] and one transposon primer (T/BAL or T/JB3) was used to validate the orientation of the transposon insertion. B6, control C57BL/6 tail gDNA; MSCV 5′LTR, long terminal repeat of the murine stem cell virus; pA, polyadenylation signal; SA, splice acceptor; SD, splice donor. (*C*) Real-time PCR quantitation of *Ncoa2* and *G6Pase* mRNA expression in four liver tumors normalized to mRNA expression of the surrounding normal liver. Bar graphs represent mean *Ncoa2* and *G6Pase* mRNA levels relative to Actin and 18S rRNA controls, respectively. Error bars represent SDs from three independent measurements.

in an independent system, we used hepatoblasts isolated from *Trp53*$^{-/-}$ mice and immortalized by MYC. These cells do not form tumors in immunocompromised mice but provide a sensitized background in which one additional genetic alteration suffices to drive tumorigenesis (13–15). Furthermore, the *Myc* retrovirus used to immortalize these liver progenitor cells coexpresses GFP, allowing fluorescence imaging of subcutaneous tumors. We modified these cells through the introduction of shRNAs corresponding to candidate genes, followed by transplantation into recipient mice (Fig. 3*A*). Using this approach, we assess directly whether loss of function of candidate genes influences tumorigenesis and, by extension, whether these genes suppress tumor initiation. As a positive control, we knocked down the Wnt signaling pathway component *Apc*, a known tumor suppressor in this system (Fig. S8*A*). We confirmed that shRNAs targeting *Apc* in *Trp53*$^{-/-}$*; Myc* hepatocytes gave rise to tumors within 1 mo after injection into nude mice (Fig. S8 *B* and *C*).

We selected five genes from our *SB* screen to evaluate in this assay. We chose to focus on genes that had not been linked previously to liver cancer and in which the mouse shRNAs were readily available from the RNAi Consortium. We tested four or five different shRNAs per gene and chose the most potent shRNAs for our in vivo validation studies (Fig. 3*B* and Fig. S9 *A* and *B*). We then infected liver progenitor cells with lentiviruses expressing these shRNAs and assayed for tumor formation. Knockdown of *Zfx*, one of the top hits from our screen, promotes tumor formation of liver progenitor cells in nude mice (Fig. 3 *C* and *D*). We also validated *Ncoa2* and *β-Dystrobrevin* (*Dtnb*) as putative tumor-suppressor genes using this approach (Fig. 3*D*). In contrast, the knockdown of two other genes represented by CISs, *Zfp189*, and *Rc3h1,* did not result in tumor formation in this assay.

Analysis of Candidate CISs in Human HCC. To determine the relevance of the CISs identified in our genetic screen to human liver cancer pathogenesis, we compared our *SB* hit list with an ex-

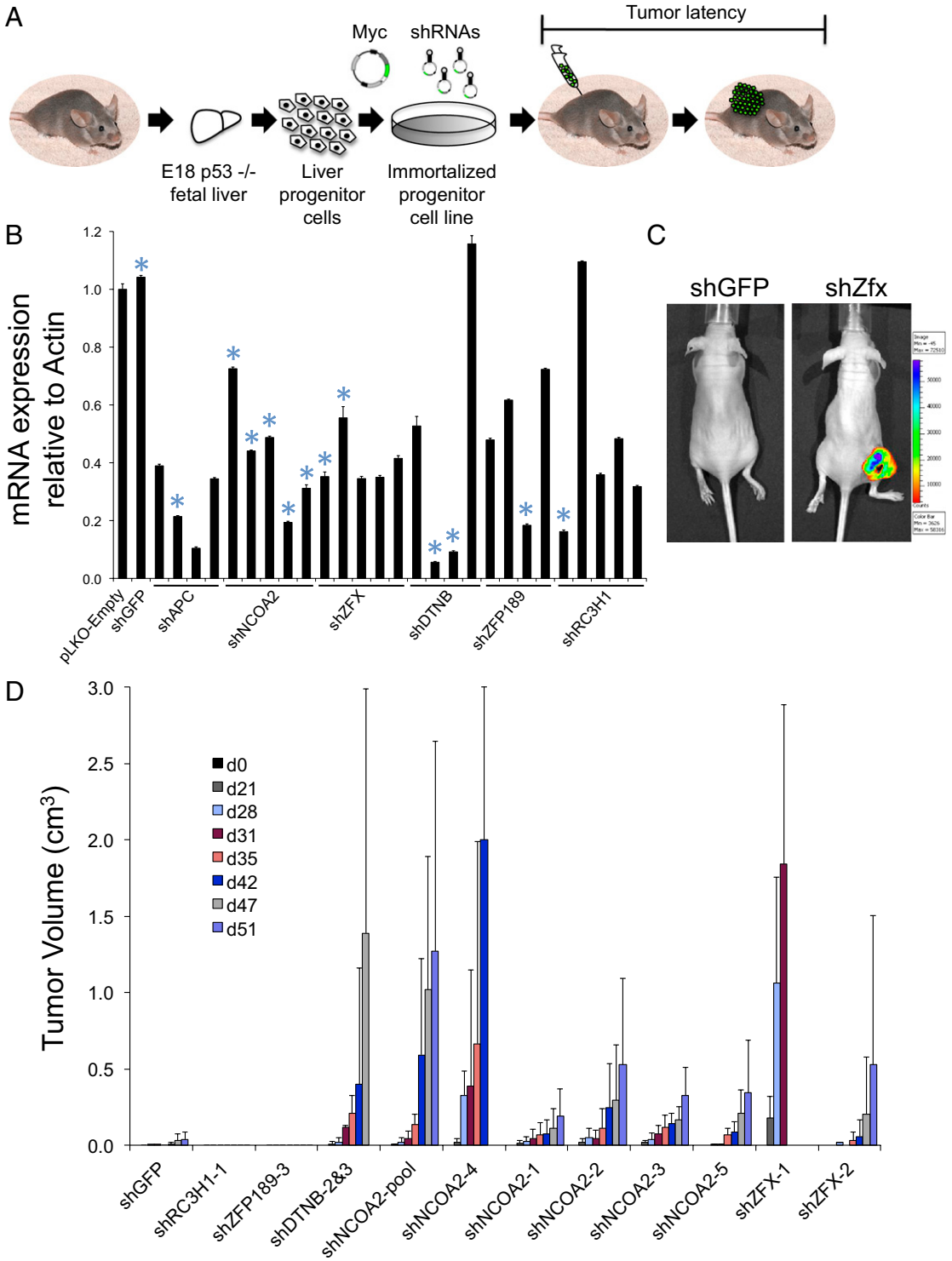

Fig. 3. Functional validation of candidate genes using a mosaic mouse model. (*A*) Overview of validation experiment. *Trp53*$^{-/-}$ hepatoblasts were immortalized with a retrovirus that expresses *Myc* and *GFP*. Cells were infected with lentiviruses expressing shRNAs that target candidate CIS genes identified in the *SB* mutagenesis screen. After selection in puromycin, cells were injected subcutaneously into nude mice, and tumor volume was measured over time. (*B*) Real-time PCR quantitation of mRNA expression after knockdown of candidate CIS genes in *Trp53*$^{-/-}$; *Myc* hepatoblasts. For every gene tested, expression of each target gene was normalized to pLKO-Empty–infected cells. Bar graphs represent mean expression levels relative to Actin. Error bars represent SDs from three independent measurements. Blue asterisks indicate shRNAs that were tested in vivo. (*C*) Fluorescence imaging of nude mice injected with liver progenitor cells expressing shRNAs corresponding to *GFP* (*Left*) and *Zfx* (*Right*). (*D*) Quantification of tumor volumes in nude mice injected with liver progenitor cells expressing candidate gene shRNAs. Bar graphs represent mean tumor volumes; error bars represent SDs from a total of four mice per shRNA tested. Independent tumorigenesis experiments yielded similar results.

tensive mRNA expression profiling dataset from a large cohort of human liver tumor samples (23). We analyzed expression of 11 orthologs of the CIS genes identified in our screen in a cohort of 139 human HCC samples. Of these, five genes were expressed at statistically significantly lower levels in human tumors than in normal human liver tissue: *ZNF608*, *NCOA2*, *CTNNA3*, *SFI1*, and *DTNB* (Fig. 4 *A* and *B*). Three genes exhibited a statistically significant increase in expression in HCC samples: *SND1*, *ZNF189*, and Wnt pathway component *BCL9* (Fig. 4 *A* and *B*).

Furthermore, we observed an association between the expression of *NCOA2* and its target *G6PC* and overall survival of HCC patients. Kaplan–Meier plot analysis and a log-rank test for overall survival in HCC based on the expression levels of these genes either independently or together revealed a statistically significant reduction in survival of HCC patients with tumors that exhibit low *NCOA2* and/or *G6PC* expression (Fig. 4*C* and Fig. S10). These findings demonstrate that our transposon-mediated forward genetic screening approach identified clinically relevant genes that participate in the pathogenesis of human liver cancer.

We next assessed whether the *NCOA2* gene accumulated sequence variants in a smaller panel of 14 human liver tumor samples. Paired normal liver biopsy material was available for a subset of these HCC samples. We sequenced all coding exons of *NCOA2* and found one potential case of loss of heterozygosity specific to the tumor (Fig. S11*A*). Consistent with deletion of one allele of *NCOA2* in this tumor, expression of *NCOA2* was reduced by 50% in this sample relative to its paired normal liver (Fig. S11*B*). In contrast, *NCOA2* expression was not decreased to the same extent in the other 13 liver tumor samples examined relative to matched normal controls (Fig. S11*C*). These results suggest that hemizygosity or other alterations affecting the *NCOA2* gene may contribute to human liver tumorigenesis.

Loss of *NCOA2* Enhances DEN-Induced Liver Tumorigenesis. To test directly whether *NCOA2* functions as a putative tumor suppressor in vivo, we treated previously described *Ncoa2*$^{+/+}$ and *Ncoa2*$^{-/-}$ mice (24) with the chemical carcinogen DEN. Exposure to DEN causes liver damage and hepatocellular carcinogenesis in mice (25, 26). We chose to analyze males because DEN-induced tumorigenesis is known to be more effective in males than in females and because males were analyzed in the original transposon screen. *Ncoa2*$^{+/+}$ and *Ncoa2*$^{-/-}$ littermate

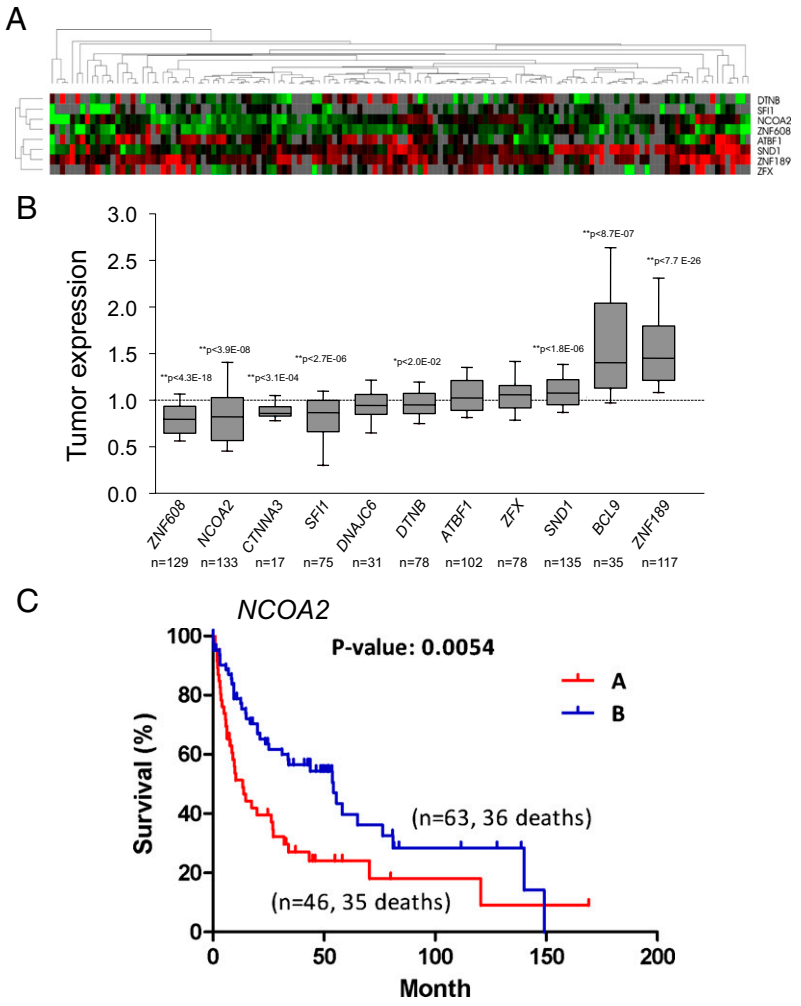

Fig. 4. Analysis of CIS candidates in human HCC samples. (*A*) Hierarchical cluster analysis of gene-expression data from 139 human HCC samples. A dendrogram (*Upper*) and heat map (*Lower*) of gene expression data were generated using eight orthologous genes from CIS candidates. Red and green cells reflect high and low expression levels, respectively; gray represents no significant information. (*B*) Quantification of tumor mRNA expression of CIS candidates relative to normal controls as previously described in Lee et al. (ref. 23). Each box represents the range of expression (25th to 75th percentile) observed. Error bars indicate the 10th and 90th percentiles, and the median is depicted by a horizontal line within the boxes. An independent one-sample *t* test was used to determine statistical significance. $*P < 0.05$; $**P < 0.01$. The *P* value and number of samples analyzed for each gene is shown. (*C*) Kaplan–Meier plots of overall survival of individuals with HCC clustered by low *NCOA2* expression (cluster A) and higher *NCOA2* expression (cluster B). $P = 0.0054$, log-rank test.

pups were injected with 25 mg/kg DEN on postnatal day 15 and then were euthanized at 3 or 6 mo postinjection. For each mouse, the liver was isolated, weighed, and photographed macroscopically (Fig. S12*A* and Table S4). DEN-treated livers were evaluated further to determine the total tumor number as well as the average and maximal tumor size. We observed that *Ncoa2*$^{-/-}$ male mice exhibited an approximately fourfold increase in tumor number and a statistically significant increase in maximal and average tumor size by 6 mo after DEN treatment ($P < 0.05$) (Fig. 5*A* and Fig. S12*B*). These findings demonstrate that genetic loss of NCOA2 promotes liver tumorigenesis in a mouse model that closely mimics human HCC pathogenesis.

Discussion

Understanding molecular mechanisms that contribute to tumor development may provide therapeutic approaches for cancer therapy. Screens using transposons facilitate the discovery of genes and pathways contributing to tumor development in mice (5, 6, 27, 28). Thus, forward genetics provides a complementary approach to cancer genome-sequencing studies by illuminating the functional relevance of genes mutated in human tumors.

We used transgenic mouse lines that express a ubiquitous transposase and a mutagenic transposon present at low copy number to screen for insertions that accelerate *MYC*-induced HCC. We found a dramatic increase in the number of quadruple-transgenic animals that developed liver tumors compared with triple-transgenic controls that also expressed the tet-*o-MYC* and LAPtTA transgenes but lacked an active *SB* transposon. Sequencing of insertions from liver tumors identified at least 16 CISs/loci that contribute to accelerated tumor development.

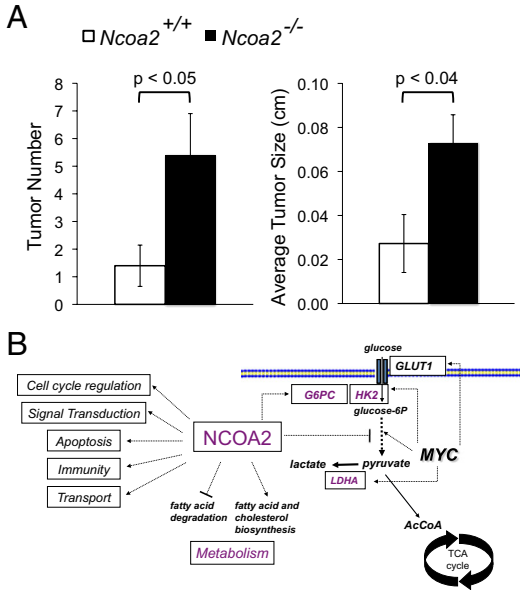

Fig. 5. Loss of Ncoa2 enhances DEN-induced liver tumorigenesis. (*A*) Quantification of liver tumor number and average liver tumor size 6 mo after DEN treatment in *Ncoa2*$^{+/+}$ and *Ncoa2*$^{-/-}$ knockout mice. Tumor number, $P = 0.04$; average tumor size, $P = 0.037$. (*B*) Model for how loss of *Ncoa2* may promote liver tumorigenesis in cooperation with *Myc*. The MYC oncogenic transcription factor reprograms metabolism in tumor cells by directly regulating genes involved in the glycolytic pathway. Loss of function of *Ncoa2* may potentiate this pathway further by modulating expression of its targets, including *G6pc* and other genes involved in glycolysis, fatty acid degradation, and cholesterol biosynthesis. Gene-expression studies have demonstrated that NCOA2 has many additional targets, including genes involved in cell-cycle regulation, signal transduction, apoptosis, immunity, and transport, which also may contribute to tumorigenesis.

Several of the CISs identified in our genetic screen have human orthologs dysregulated in human liver cancer. The genes *ZNF608*, *NCOA2*, *CTNNA3*, *SFI1*, and *DTNB* were all expressed at statistically significantly lower levels in human HCC samples. Our validation studies in *p53*$^{-/-}$; *Myc* liver progenitor cells further demonstrated that inhibition of *Ncoa2* and *Dtnb* can promote tumor formation in immunocompromised mice. DTNB, a member of the dystrobrevin protein family originally identified as components of the dystrophin–glycoprotein complex, is expressed in nonmuscle tissues including the liver, kidney, and brain (29). *Dtnb* may have previously unrecognized antitumorigenic activities. Interestingly, DTNB interacts with cAMP-dependent PKA and is proposed to play a scaffolding role in intracellular signal-transduction pathways (30). *Atbf1*, which encodes AT-motif binding factor-1 protein, also was identified in our screen. Also known as "zinc-finger homeobox 3" (ZFHX3), this protein has been shown previously to negatively regulate the expression of the liver tumor marker α-fetoprotein (*AFP*) in hepatocytes (31). Moreover, it was demonstrated previously that *ATBF1* expression was significantly reduced in 55 of 76 HCC samples (32).

We also validated the tumor-suppressor activity of *Zfx*, encoding an X-linked pluripotency-associated zinc finger transcription factor that controls the self-renewal of embryonic and hematopoietic stem cells (33), as well as B-cell proliferation (34), in our functional studies. Although ZFX has not been linked previously to human liver tumors, and we did not observe altered expression of this gene in HCC samples, a potential link between the transcriptional networks coregulated by MYC and ZFX was discovered recently. A strong correlation in target gene occupancy was identified between these transcription factors (35). Transcriptional targets of these proteins are enriched for genes involved in the cell cycle, cell death, and cancer. Although future studies are necessary to elucidate the functional relationship between ZFX and MYC, previous findings and those reported here suggest that ZFX may directly oppose the activity of MYC at key transcriptional targets. Loss of *ZFX* may therefore remove an important negative regulator of MYC-mediated transactivation of oncogenic targets.

Genes with human orthologs that show increases in the level of mRNA expression in human liver tumor samples include *SND1*, *ZNF189*, and the Wnt pathway component *BCL9*. Dysregulation of the Wnt signaling pathway is a key molecular lesion in liver cancer (36–38). More than 60% of liver tumors exhibit accumulation of β-catenin, a hallmark of activated Wnt signaling. Interestingly, *BCL9* was shown previously to be required for β-catenin–mediated transcriptional activity in human cancer cell lines (39). Recent findings suggest that *BCL9* is an oncogene, because it has been shown to increase cell proliferation, migration, invasion, and metastatic potential of tumor cells (40). One additional gene identified in our screen, *Ctnna3*, also interacts with the Wnt pathway (41). Further analysis of all CIS genes using the COSMIC database analysis revealed the presence of additional mutations and/or genomic alterations that may be relevant to the pathogenesis of diverse human tumor types (Table S5). In light of the data presented here, these variants are worthy of further investigation.

An independent *SB* mutagenesis screen using a dominant-negative *Trp53* transgene recently identified 19 genes associated with liver cancer (5). Interestingly, the only CIS gene in common between this study and the Keng study was *Sfi1* (5). A meta-analysis of several *SB* screens indicates that this gene scores very highly in many such screens. Recent work suggests that this finding reflects an artifact caused by previously unrecognized amplification of this gene through segmental duplications and/or other mechanisms in the C57BL/6 mouse genome (42). Nevertheless, we found that *SFI1* mRNA expression was down-regulated in a panel of 139 human HCC samples. Consistent with this result, Keng et al. (5) found distinct copy-number losses of *SFI1* in 20 of 28 human HCC samples examined. *SFI1* is a centrosomal protein with well-studied homologs present in yeast. Although SFI1 has been proposed to

play a role in the formation of centrosome-associated contractile fibers (43), and the data presented here and in Keng et al. (ref. 5) are most consistent with a potential tumor-suppressive role for SFI1, additional studies are needed to determine the role of this gene in chromosome stability and to elucidate how its reduced expression may contribute to tumorigenesis.

Transposon insertions in *Egfr* were very common in liver tumors isolated from mice harboring a dominant-negative *Trp53* transgene and a conditional *SB* transposase (5). In fact, *SB* insertions were detected most frequently in intron 24 of *Egfr*, giving rise to a truncated Egfr protein that has a strongly oncogenic effect. Using a PCR genotyping assay, we screened all liver tumors isolated in our genetic screen and did not find a single occurrence of *SB* insertions in this intron. Presumably, MYC overexpression performs a function that obviates selection for *Egfr* activation in this model, perhaps because EGFR signaling results in MYC upregulation through the RAS–RAF–MEK–MAPK pathway (44, 45). Moreover, this finding underscores the importance of performing screens of this type using multiple sensitized models, because the most relevant pathways in a given tumor may depend on the initiating event that drives tumorigenesis.

Perhaps most intriguing, our findings provide evidence that the transcriptional coactivator NCOA2 acts as a tumor suppressor in liver cancer. Four lines of data support this concept. (*i*) Recurrent transposon insertions in *SB*-induced liver tumors result in decreased mRNA expression of both *Ncoa2* and its previously characterized target *G6pc*. (*ii*) Inhibition of *Ncoa2* using multiple independent shRNAs promotes tumor formation of liver progenitor cells in immunocompromised mice. (*iii*) DEN treatment of *Ncoa2* $^{-/-}$ mice enhances liver tumorigenesis compared with *Ncoa2*$^{+/+}$ littermates. (*iv*) Decreased expression of *NCOA2* is observed in human liver tumor samples.

Previous studies of *Ncoa2* illuminate our mechanistic understanding of its tumor-suppressor activity. Mice lacking *Ncoa2* develop glycogen storage disease type 1 (Von Gierke's disease) and exhibit decreased expression and enzymatic activity of G6pase (21). Similarly, a genetic deficiency of *G6PC* leads to Von Gierke's disease both in humans and in mice (46, 47). Several observations demonstrate that loss of function of G6Pase also promotes liver tumorigenesis. For example, enzymatic activity of G6Pase is reduced in human and rodent liver tumors (48, 49), and *G6pc*$^{-/-}$ mice develop hepatic tumors (47). Furthermore, a significant fraction of patients with glycogen storage disease type 1 develop hepatic adenomas and have an additional risk of undergoing malignant transformation (50). Finally, inhibition of hexokinase, which has the equivalent functional effect as increasing G6Pase activity, is antitumorigenic (51, 52).

Based on these findings, loss of *Ncoa2* may promote liver tumorigenesis at least in part through a subsequent reduction in G6Pase activity (Fig. 5*B*). This reduction, in turn, may increase the intracellular pool of glucose-6-phosphate that can enter the glycolytic pathway. Our data indicate that loss of *Ncoa2* is particularly protumorigenic in settings of MYC hyperactivity, which is consistent with the known ability of MYC to stimulate glycolytic metabolism potently through the direct induction of expression of numerous genes in the glycolytic pathway (53–55). Despite the potential relevance of this mechanism to tumorigenesis, we were unable to detect expression of G6Pase in the hepatoblast cells, suggesting that NCOA2 tumor-suppressor activity is independent of G6Pase in the hepatoblast system. Although this finding does not rule out the potential significance of G6Pase as a relevant target of NCOA2 in vivo, we acknowledge that mechanisms of NCOA2-mediated tumor suppression are complex and likely involve multiple targets and pathways. Indeed, a previously reported microarray analysis of gene expression in livers of *Ncoa2*$^{-/-}$ mice revealed a signature of increased energy expenditure including the stimulation of genes involved in fatty acid degradation and suppression of genes involved in cholesterol and fatty acid biosynthesis (22). Thus, *Ncoa2* deficiency likely contributes to a broader protumorigenic reprogramming of metabolism beyond the glycolytic pathway. Moreover, loss of function of *Ncoa2* influences gene-expression programs relevant to other important aspects of tumor biology including cell-cycle regulation, signal transduction, and apoptosis. Therefore future studies are warranted to further dissect the mechanism(s) by which dysregulated expression of NCOA2 contributes to tumorigenesis.

Methods

Transgenic Animals. LAPtTA and tet-*o-MYC* mice were obtained from Dean Felsher (Stanford School of Medicine, Stanford, CA). T2/Onc transgenic mice with the donor concatemer on chromosome 15 were bred with LAPtTA mice to obtain T2/Onc; LAPtTA animals. Simultaneously, *Rosa26-SB11* females were bred to tet-*o-MYC* males to obtain *Rosa26-SB11*; tet-*o-MYC* mice. The two double-transgenic lines were first intercrossed with littermates to produce homozygous transgenes when possible. In the final cross, LAPtTA; T2/Onc females were bred with *Rosa26-SB11*; tet-*o-MYC* males to obtain quadruple (experimental) or triple (control) transgenic cohorts. The *MYC* transgene is on chromosome Y, precluding analysis of females. The Johns Hopkins Animal Care and Use Committee approved all procedures described in this work.

PCR Genotyping. Genomic DNA was isolated from tail clippings using the DNeasy Blood and Tissue Kit (Qiagen) according to the manufacturer's instructions. PCR genotyping was performed using 10–100 ng of genomic DNA as template. Primers used were tet-*o-MYC*, forward 5′-TAGTGAACCGTCAGATCGCCTG-3′ and reverse 5′-TTTGATGAAGGTCTCGTCGTCC-3′ (amplicon 500 bp); LAPtTA, forward 5′-GCTGCTTAATGAGGTCGG-3′ and reverse 5′-CTCTGCACCTTGGTGATC-3′ (amplicon 500 bp); T2/Onc, forward 5′-CCTTGCAAAATGGCGTTACT-3′ and reverse 5′-GCCGCACTGGTTGTTAGCAA-3′ (amplicon 200 bp); *Rosa26-SB11* WT, forward 5′-CTGTTTTGGAGGCAGGAA-3′, reverse 5′-CCCCAGATGACTACCTATCCTCCC-3′ (amplicon 420 bp); *Rosa26-SB11* SB reverse 5′-CTAAAAGGCCTATCACAAAC-3′ (SB knock in amplicon 317 bp); *Hprt*, forward 5′-CTTTCTTGTCACTCCCACTTTTCC-3′ and reverse 5′-CACATCCTTCATTCAGGTGTCACT-3′ (amplicon 340 bp). PCR conditions for Ex Taq (Takara) were used according to the manufacturer's instructions. PCR products were separated on a 1.2% agarose gel.

Liver Tumor Analysis. The whole liver was dissected from the euthanized animal, washed, and placed in ice-cold PBS. The number of liver tumor nodules was counted for each animal. Tumor nodules then were dissected away from surrounding normal liver tissue. When large enough, tumor nodules were split into three pieces for gDNA isolation, RNA isolation, and histological analysis. DNA isolation was performed using the All-in-One Purification Kit (Norgen) or by phenol-chloroform extraction. Total RNA was isolated from tumor and normal tissue using TRIzol (Invitrogen) followed by additional cleanup and DNase digestion using the RNeasy kit (Qiagen) according to the manufacturers' protocols. For histological analysis, tissues were fixed in 10% formalin, embedded in paraffin, and sectioned. Tissue section slides then were stained with H&E using standard protocols.

SB Excision Assay. To confirm excision of the T2/Onc transgene from the chromosome 15 concatemer, we used the following forward 5′-TGTGCTGCAAGGCGATTA-3′ and reverse 5′-ACCATGATTACGCCAAGC-3′ primers (amplicon 233 bp); *Gapdh*, forward 5′-GGAGCCAAACGGGTCATCATCTC-3′ and reverse 5′-GAGGGGCCATCCACAGTCTTCT-3′. PCR conditions for Ex Taq (Takara) were used according to the manufacturer's instructions. PCR products were separated on a 1.2% agarose gel.

***Ncoa2* Insertion Validation Assay.** For each insertion that was validated, 1 kb of sequence surrounding each insertion position was downloaded (500 bp on each side of the insertion), and an ~800-bp amplicon was designed. To confirm the orientation of the *SB* insertion, different combinations of *Ncoa2* and T2/Onc primers were used in the PCR. Primers used to confirm *SB* insertion at position 13272606 were forward 5′-CACACACACACACAGCAGTAGTGAAGCA-3′ and reverse 5′-CGCCAGAAAACTGATTTTGAAGTTGCAG-3′; to confirm the *SB* insertion at position 13300371, the primers used were forward 5′-GAGCGATGGTTTCTACTCCCACAGACCT-3′ and reverse 5′- CTGTACCGTGGTGAGCATTGGGAGTAAT-3′.

Sequence Processing and Annotation. The 47,343 initial 454 sequencing reads were processed and analyzed using a custom semiautomated processing

pipeline first described in ref. 6. Briefly, Fasta-formatted sequences from 454 runs were assigned to libraries allowing one mismatch in the 10-bp barcode. All raw sequences were scanned for inverted repeat/direct repeat (IRDR) and linker recognition sequences using EMBOSS Vectorstrip (56) with successively less stringent parameters (10%, 15%, and finally 20% mismatches allowed) until the maximum number of constructs (i.e., IRDR: GTGTATGTAAACTTCCGACTTCAACTG and linker sequence: GTCCCTTAAGCGGAGCCCT) were recognized and trimmed off. Only 44,294 sequences that had a matched IRDR with an insert sequence of at least 16 bp were carried further for mapping to the mouse genome. These trimmed insert sequences were mapped to the mouse genome (National Center for Biotechnology Information build 37) using BLASTN (DeCypher's TeraBLASTN; Active Motif), requiring query sequences to align within 1 bp of the end of the LTR sequence that was trimmed. Additionally, the query sequence was required to match with at least 95% identity. Ambiguous sequences that mapped to multiple genomic loci were removed, leaving 2,090 uniquely mappable nonredundant insertions. Unambiguously mapped nonredundant insertions were assigned to clusters of CISs if the local density of insertions in a given window size exceeded the density that would be expected by chance, as determined by Monte Carlo simulation. A CIS is defined as statistically significant if a region in the genome has three or more *SB* insertions with a 30-kb window or four or more insertions within 155 kb. CISs that occurred at the same nucleotide in different tumors from the same mouse were removed with the exceptions of *Zfp608* and *Bcl9*. Nonredundant insertion positions were annotated using the EnsEMBL API (57) with the name of the gene whose start site was closest to the position. CIS positions were annotated similarly using the median insertion position within the CIS as a reference point.

Bioinformatic Analysis of SB Insertions. To analyze mouse genomic features that harbor SB insertions, additional computational analysis was performed using the Python programming language (www.python.org) and the R statistical environment (http://www.R-project.org/).

Cell Culture. HEK293T and *Trp53* $^{-/-}$*; Myc* cells were cultured in high-glucose (4.5 g/L) DMEM supplemented with 10% FBS, penicillin, and streptomycin.

Lentiviral Infection of PHM Cells. HEK293T (1×10^6) cells were cotransfected with pLKO shRNA constructs, Gag/Pol, VSV-G, and Rev helper plasmids using the FuGene6 reagent (Roche). Following transfection, the lentiviral supernatant was collected, filtered, and supplemented with 8μg/mL hexadimethrene bromide (Sigma). *Trp53*$^{-/-}$; Myc cells (1×10^5) were infected overnight twice and, 24 h after the second infection, were plated into medium containing 1.5 μg/mL puromycin and selected for at least 7 d. Cells then were injected into nude mice and harvested for RNA analysis. The following TRC clone IDs were used for knockdown experiments: *Apc*: (B4) TRCN0000042533, (B5) TRCN0000042534, (B6) TRCN0000042535, (B7) TRCN0000042536; *Ncoa2*: (*i*) TRCN0000096169, (*ii*) TRCN0000096170, (*iii*) TRCN0000096171, (*iv*) TRCN0000096172, (*v*) TRCN0000096173; Zfx: (*i*) TRCN0000095620, (*ii*) TRCN0000095619, (*iii*) TRCN0000095621, (*iv*) TRCN0000095622, (*v*) TRCN0000095623; Dtnb: (*i*) TRCN0000108760, (*ii*) TRCN0000108761, (*iii*) TRCN0000108762, (*iv*), TRCN0000108764; Zpf189: (*i*) TRCN00000082103, (*ii*) TRCN0000082105, (*iii*) TRCN0000082106, (*iv*) TRCN0000082107; Rc3h1: (*i*) TRCN0000200305; (*ii*) TRCN0000177880, (*iii*) TRCN0000198362, (*iv*) TRCN0000200175, (*v*) TRCN0000177150.

RT-PCR Analysis of CIS Genes. All quantitative real-time PCR analysis was performed using the Step One Plus Real Time PCR system (Applied Biosystems). Analysis of *Ncoa2* in *SB* liver tumors was performed using a predeveloped TaqMan assay with One-Step RT-PCR Master Mix Reagents (Applied Biosystems) or by SYBR green analysis of cDNA samples using primers that cross an exon–exon junction. The *Ncoa2* TaqMan assay was performed with Mm00500749_m1 (Applied Biosystems). Primers used for SYBR green were forward 5′-TCACTGCATTGGCTCTTCTG-3′ and reverse 5′-TGTTTTCTCCCATCCCACTC-3′. Analysis of *G6Pase* mRNA in *SB* liver tumors was performed with a TaqMan assay using the Universal Probe #26 (Roche) and forward 5′-GAGGAAAGAAAAAGCCAACGTA-3′ and reverse 5′-GGGACAGACAGACGTTCAGC-3′ primers. Expression was normalized to 18SrRNA with the Ribosomal RNA control assay (Applied Biosystems) or *Actin*. All PCR assays were performed in triplicate.

To assess the efficiency of shRNAs in *Trp53*$^{-/-}$; Myc cells, RNA was isolated from cell pellets using the RNeasy Kit (Qiagen), and 2 μg total RNA was reverse transcribed using SuperScript III First Strand (Invitrogen) according to the manufacturers' protocols. SYBR green analysis was performed with cDNA samples using primers that cross exon–exon junctions for each gene. Primers used for *Apc* were forward 5′-AAGACGGTATGCTGGAATGG-3′ and reverse 5′-AGTGCTCTCATGCAGCCTTT-3′; *Ncoa2* forward 5′-TGGACATGATCAAGCAGGAG-3′ and reverse 5′-CCCAGTGGGTTGAAGAAAGA-3′; *Zfx* forward 5′-CGGCAGACTGGCTAAACAA-3′ and reverse 5′-CCACAAATCATGCAAGGGTA-3′; *Dtnb* forward 5′-CATGTGTGGTGGAAAAATGC-3′ and reverse 5′-CCTTCAGGAACTGGTCAAGC-3′; *Zfp189* forward 5′-GGCTGCTATTCCTGAACGAG-3′ and reverse 5′-AGGCTTCTCGGAGCTGGAT-3′; *Rc3h1* forward 5′-GCAGCTGAACCATCAGATCA-3′ and reverse 5′-GGGTGTTCACCTCCCTCTGT-3′; *Actin* forward 5′-CGGTTCCGATGCCCTGAGGCTCTT-3′ and reverse 5′-CGTCACACTTCATGATGGAATTGA-3′. All SYBR green PCR assays were performed in triplicate.

Xenograft Assay. *Trp53*$^{-/-}$*; Myc* cells (2×10^6) expressing shRNA lentiviruses were injected subcutaneously into the right flank of 6- to 8-wk-old female nude mice (National Cancer Institute-Frederick). Tumor volume was measured with calipers every 3–5 d until the average tumor mass reached 2 cm^3. Tumor volume was calculated with the formula (length × width^2)/2. A total of four mice were injected per shRNA tested. At least two independent tumorigenesis experiments were performed for each gene.

GFP Imaging. Whole-body GFP imaging was performed using the IVIS Spectrum Optical Imaging system (Xenogen) according to the manufacturer's instructions.

Microarray Analysis of Human HCC Samples. The mRNA expression data of 12 genes in human HCC were obtained from Gene Expression Omnibus with accession nos. GSE4024 and GSE1898 (23). Hierarchical cluster analysis was conducted using Cluster 3.0, and the image analysis was performed with TreeView 1.60 software (Michael Eisen Laboratory, Lawrence Berkeley National Laboratory and University of California, Berkeley, CA; http://rana.lbl.gov/eisen/). We applied Kaplan–Meier plot analysis and a log rank test for overall survival in HCC by using Prism v. 5.03 (GraphPad Software, Inc.).

DEN Tumorigenesis Experiment. Fifteen-day-old male *Ncoa2*$^{+/+}$ and *Ncoa2*$^{-/-}$ littermate pups were injected intraperitoneally with a 25 mg/kg dose of DEN (Sigma) in 0.9% sterile saline as previously described (58). DEN-treated mice were fed normal chow (Teklad 2920×) and euthanized at 3 or 6 mo postinjection. Mice were weighed, and liver was isolated, weighed, and photographed macroscopically. Livers were evaluated further to determine the total number of tumors as well as average and maximal tumor size using a handheld micrometer. Samples of liver tissue were prepared for histological analysis as previously described (59).

ACKNOWLEDGMENTS. We thank Dean Felsher for tet-o-*MYC* and LAPtTA mice; Scott Lowe for *Trp53* $^{-/-}$*; Myc* liver progenitor cells; Adam Dupuy, Nancy Jenkins, and Neal Copeland for *Rosa26-SB11* mice; Eric Cooper for Gag/Pol, Rev, and VSV-G helper plasmids; and J. Mendell and C. Dang for critical reading of the manuscript. The Minnesota Supercomputing Institute provided system administration support and the computational research infrastructure used to perform the analysis. This work was supported by National Institutes of Health Grant CA16519 (to J.D.B.) and National Cancer Institute Grant R01CA113535 (to D.A.L.). K.A.O. was a Damon Runyon fellow supported by the Damon Runyon Cancer Research Foundation Grant DRG-1918-06 and currently is a Cancer Prevention Research Institute of Texas Scholar in Cancer Research.

1. Ivics Z, Hackett PB, Plasterk RH, Izsvák Z (1997) Molecular reconstruction of Sleeping Beauty, a Tc1-like transposon from fish, and its transposition in human cells. *Cell* 91: 501–510.
2. Collier LS, Carlson CM, Ravimohan S, Dupuy AJ, Largaespada DA (2005) Cancer gene discovery in solid tumours using transposon-based somatic mutagenesis in the mouse. *Nature* 436:272–276.
3. Dupuy AJ, Akagi K, Largaespada DA, Copeland NG, Jenkins NA (2005) Mammalian mutagenesis using a highly mobile somatic Sleeping Beauty transposon system. *Nature* 436:221–226.
4. Collier LS, et al. (2009) Whole-body sleeping beauty mutagenesis can cause penetrant leukemia/lymphoma and rare high-grade glioma without associated embryonic lethality. *Cancer Res* 69:8429–8437.
5. Keng VW, et al. (2009) A conditional transposon-based insertional mutagenesis screen for genes associated with mouse hepatocellular carcinoma. *Nat Biotechnol* 27:264–274.
6. Starr TK, et al. (2009) A transposon-based genetic screen in mice identifies genes altered in colorectal cancer. *Science* 323:1747–1750.
7. Roberts LR (2008) Sorafenib in liver cancer—just the beginning. *N Engl J Med* 359: 420–422.

8. Thorgeirsson SS, Grisham JW (2002) Molecular pathogenesis of human hepatocellular carcinoma. *Nat Genet* 31:339–346.
9. Buendia MA (2000) Genetics of hepatocellular carcinoma. *Semin Cancer Biol* 10:185–200.
10. Beer S, et al. (2004) Developmental context determines latency of MYC-induced tumorigenesis. *PLoS Biol* 2:e332.
11. Felsher DW, Bishop JM (1999) Reversible tumorigenesis by MYC in hematopoietic lineages. *Mol Cell* 4:199–207.
12. Shachaf CM, et al. (2004) MYC inactivation uncovers pluripotent differentiation and tumour dormancy in hepatocellular cancer. *Nature* 431:1112–1117.
13. Zender L, et al. (2006) Identification and validation of oncogenes in liver cancer using an integrative oncogenomic approach. *Cell* 125:1253–1267.
14. Zender L, et al. (2005) Generation and analysis of genetically defined liver carcinomas derived from bipotential liver progenitors. *Cold Spring Harb Symp Quant Biol* 70: 251–261.
15. Zender L, et al. (2008) An oncogenomics-based in vivo RNAi screen identifies tumor suppressors in liver cancer. *Cell* 135:852–864.
16. Keng VW, et al. (2005) Region-specific saturation germline mutagenesis in mice using the Sleeping Beauty transposon system. *Nat Methods* 2:763–769.
17. Carlson CM, et al. (2003) Transposon mutagenesis of the mouse germline. *Genetics* 165:243–256.
18. Horie K, et al. (2003) Characterization of Sleeping Beauty transposition and its application to genetic screening in mice. *Mol Cell Biol* 23:9189–9207.
19. Vigdal TJ, Kaufman CD, Izsvák Z, Voytas DF, Ivics Z (2002) Common physical properties of DNA affecting target site selection of sleeping beauty and other Tc1/mariner transposable elements. *J Mol Biol* 323:441–452.
20. García-Caballero T, et al. (2000) Increased expression of growth hormone and prolactin receptors in hepatocellular carcinomas. *Endocrine* 12:265–271.
21. Chopra AR, et al. (2008) Absence of the SRC-2 coactivator results in a glycogenopathy resembling Von Gierke's disease. *Science* 322:1395–1399.
22. Jeong JW, et al. (2006) The genomic analysis of the impact of steroid receptor coactivators ablation on hepatic metabolism. *Mol Endocrinol* 20:1138–1152.
23. Lee JS, et al. (2006) A novel prognostic subtype of human hepatocellular carcinoma derived from hepatic progenitor cells. *Nat Med* 12:410–416.
24. Gehin M, et al. (2002) The function of TIF2/GRIP1 in mouse reproduction is distinct from those of SRC-1 and p/CIP. *Mol Cell Biol* 22:5923–5937.
25. Fausto N, Campbell JS (2010) Mouse models of hepatocellular carcinoma. *Semin Liver Dis* 30:87–98.
26. Maeda S, Kamata H, Luo JL, Leffert H, Karin M (2005) IKKbeta couples hepatocyte death to cytokine-driven compensatory proliferation that promotes chemical hepatocarcinogenesis. *Cell* 121:977–990.
27. Rad R, et al. (2010) PiggyBac transposon mutagenesis: A tool for cancer gene discovery in mice. *Science* 330:1104–1107.
28. Starr TK, et al. (2011) A Sleeping Beauty transposon-mediated screen identifies murine susceptibility genes for adenomatous polyposis coli (Apc)-dependent intestinal tumorigenesis. *Proc Natl Acad Sci USA* 108:5765–5770.
29. Loh NY, Nebenius-Oosthuizen D, Blake DJ, Smith AJ, Davies KE (2001) Role of beta-dystrobrevin in nonmuscle dystrophin-associated protein complex-like complexes in kidney and liver. *Mol Cell Biol* 21:7442–7448.
30. Ceccarini M, et al. (2007) Association of dystrobrevin and regulatory subunit of protein kinase A: A new role for dystrobrevin as a scaffold for signaling proteins. *J Mol Biol* 371:1174–1187.
31. Yasuda H, Mizuno A, Tamaoki T, Morinaga T (1994) ATBF1, a multiple-homeodomain zinc finger protein, selectively down-regulates AT-rich elements of the human alpha-fetoprotein gene. *Mol Cell Biol* 14:1395–1401.
32. Kim CJ, et al. (2008) Down-regulation of ATBF1 is a major inactivating mechanism in hepatocellular carcinoma. *Histopathology* 52:552–559.
33. Galan-Caridad JM, et al. (2007) Zfx controls the self-renewal of embryonic and hematopoietic stem cells. *Cell* 129:345–357.
34. Arenzana TL, Smith-Raska MR, Reizis B (2009) Transcription factor Zfx controls BCR-induced proliferation and survival of B lymphocytes. *Blood* 113:5857–5867.
35. Hu G, et al. (2009) A genome-wide RNAi screen identifies a new transcriptional module required for self-renewal. *Genes Dev* 23:837–848.
36. Lee HC, Kim M, Wands JR (2006) Wnt/Frizzled signaling in hepatocellular carcinoma. *Front Biosci* 11:1901–1915.
37. Merle P, et al. (2005) Oncogenic role of the frizzled-7/beta-catenin pathway in hepatocellular carcinoma. *J Hepatol* 43:854–862.
38. Satoh S, et al. (2000) AXIN1 mutations in hepatocellular carcinomas, and growth suppression in cancer cells by virus-mediated transfer of AXIN1. *Nat Genet* 24: 245–250.
39. de la Roche M, Worm J, Bienz M (2008) The function of BCL9 in Wnt/beta-catenin signaling and colorectal cancer cells. *BMC Cancer* 8:199.
40. Mani M, et al. (2009) BCL9 promotes tumor progression by conferring enhanced proliferative, metastatic, and angiogenic properties to cancer cells. *Cancer Res* 69: 7577–7586.
41. Busby V, et al. (2004) Alpha-T-catenin is expressed in human brain and interacts with the Wnt signaling pathway but is not responsible for linkage to chromosome 10 in Alzheimer's disease. *Neuromolecular Med* 5:133–146.
42. Quinlan AR, et al. (2010) Genome-wide mapping and assembly of structural variant breakpoints in the mouse genome. *Genome Res* 20:623–635.
43. Martinez-Sanz J, et al. (2006) Binding of human centrin 2 to the centrosomal protein hSfi1. *FEBS J* 273:4504–4515.
44. Downward J (2003) Targeting RAS signalling pathways in cancer therapy. *Nat Rev Cancer* 3:11–22.
45. Soucek L, et al. (2008) Modelling Myc inhibition as a cancer therapy. *Nature* 455: 679–683.
46. Chou JY, Matern D, Mansfield BC, Chen YT (2002) Type I glycogen storage diseases: Disorders of the glucose-6-phosphatase complex. *Curr Mol Med* 2:121–143.
47. Mutel E, et al. (2011) Targeted deletion of liver glucose-6 phosphatase mimics glycogen storage disease type 1a including development of multiple adenomas. *J Hepatol* 54:529–537.
48. Tsubouchi H, Kamibeppu A, Fujisaki K, Nagahama J, Hashimoto S (1980) Hepatic gluconeogenic key enzymes in patients with hepatic cancer. *Gastroenterol Jpn* 15: 564–569.
49. Weber G, Cantero A (1955) Glucose-6-phosphatase activity in normal, pre-cancerous, and neoplastic tissues. *Cancer Res* 15:105–108.
50. Lee PJ (2002) Glycogen storage disease type I: Pathophysiology of liver adenomas. *Eur J Pediatr* 161(Suppl 1):S46–S49.
51. Kim W, et al. (2007) Apoptosis-inducing antitumor efficacy of hexokinase II inhibitor in hepatocellular carcinoma. *Mol Cancer Ther* 6:2554–2562.
52. Pelicano H, Martin DS, Xu RH, Huang P (2006) Glycolysis inhibition for anticancer treatment. *Oncogene* 25:4633–4646.
53. Kim JW, et al. (2004) Evaluation of myc E-box phylogenetic footprints in glycolytic genes by chromatin immunoprecipitation assays. *Mol Cell Biol* 24:5923–5936.
54. Shim H, et al. (1997) c-Myc transactivation of LDH-A: Implications for tumor metabolism and growth. *Proc Natl Acad Sci USA* 94:6658–6663.
55. Osthus RC, et al. (2000) Deregulation of glucose transporter 1 and glycolytic gene expression by c-Myc. *J Biol Chem* 275:21797–21800.
56. Rice P, Longden I, Bleasby A (2000) EMBOSS: The European Molecular Biology Open Software Suite. *Trends Genet* 16:276–277.
57. Stabenau A, et al. (2004) The Ensembl core software libraries. *Genome Res* 14: 929–933.
58. Sakurai T, Maeda S, Chang L, Karin M (2006) Loss of hepatic NF-kappa B activity enhances chemical hepatocarcinogenesis through sustained c-Jun N-terminal kinase 1 activation. *Proc Natl Acad Sci USA* 103:10544–10551.
59. York B, et al. (2010) Reprogramming the posttranslational code of SRC-3 confers a switch in mammalian systems biology. *Proc Natl Acad Sci USA* 107:11122–11127.